Int. J. Heat Mass Transfer. Vol. 35, No. 11, pp. 2795–2803, 1992
Printed in Great Britain

0017–9310/92 $5.00+0.00

Solidification of arbitrarily shaped casting in mold–casting system

R. Y. TZONG and S. L. LEE

Department of Power Mechanical Engineering, National Tsing-Hua University, Hsinchu, Taiwan 30043, Republic of China

(*Received* 3 *January* 1991 *and in final form* 23 *January* 1992)

Abstract—In the present investigation, an enthalpy formulation is applied to the solidification process of an arbitrarily shaped casting in a mold–casting system. The effect of thermal contact resistance existing at the mold–casting interface is also studied. All of the computations are performed on a Cartesian coordinate system without recourse to coordinate transformation or grid generation for the arbitrary shape of the mold–casting interface. A single region method based on the weighting function scheme is found to solve this mold–casting conjugate heat transfer problem quite efficiently. A few cases are conducted to study the effects of the Stefan number, the thermophysical properties and the thermal contact resistance (at the mold–casting interface) on the solidification processing. The numerical result of the moving solidification front is investigated for each case. To examine the performance of the present numerical technique in a particular respect, chill blocks are employed at some locations inside the mold such that more than one isolated liquid region could exist in the casting during the solidification processing. Even for such a 'multiple-region' problem, the present numerical method shows good performances. No additional computational effort is needed as compared with the cases without chill blocks.

INTRODUCTION

HEAT TRANSFER problems dealing with solidification of an arbitrarily shaped casting in a mold–casting system are encountered in many foundry practices such as the sand-mold casting and the die casting processes. In these casting processes, a molten metal is fed into a cavity having a specified geometry to produce a solid object with the desired shape upon solidification. It is well known that the heat transfer mechanism in the solidification process has a significant effect on the microstructure of the casting, the stripping time and the generation of residual thermal stress, etc. Unfortunately, the heat transfer phenomenon in casting processing is very difficult to observe from experimental studies due to the opaqueness and high melting point that most metals have. Under such a situation, numerical simulations have received considerable attention during the past decades. However, most of the techniques that have been developed for solidification problems such as those in refs. [1–9] pose numerical instability even for rectangular casting 'without' mold. A detailed discussion on this point can be found in ref. [10].

In mold–casting systems, there are three regions (namely, the mold, the solidified metal and the molten metal) in the entire physical domain in the course of the solidification process. Under practical situations, all of these regions possess arbitrary shapes. To adapt to the complex geometries, grid generation techniques have been employed by many previous investigators. For instance, Kroeger and Ostrach [11] used the method of conformal mapping to generate grid systems for each of the solid and liquid regions in a continuous casting process. Gilmore and Guceri [12] obtained grid systems for an angle bend and a ply drop by using Poisson equations. However, these methods are very complex especially when the casting possesses a highly sinuous shape. To simplify the computations, the influence of the mold on the casting is estimated through the use of a boundary condition imposed on the mold–casting interface [11–13] instead of solving the heat conduction inside the mold. This treatment will undoubtedly introduce significant errors into the solution. In some commercial computer codes, both regions of casting and mold are approximated with brick-type mesh [14–16] such that computations can be performed on a Cartesian coordinate system. However, this approximation is restricted to the use of small grids.

Generally speaking, the thermophysical properties are different in the above-mentioned three regions. Without particular treatment, the thermophysical property jumps existing at the interface of these regions would cause serious numerical instability. This situation will be even worse when the mold–casting interface has an arbitrary shape. In addition, the shrinkage of the casting and/or the thermal expansion of the mold during the solidification process would form gaps at the mold–casting interface. This gives rise to considerable thermal contact resistance. All of these facts render the numerical computations very difficult when solving the solidification problem of mold–casting systems. Fortunately, the weighting function scheme proposed in ref. [10] solves problems with discontinuous thermophysical properties. In the use of this particular numerical scheme, the temperatures at the grid points are directly related to the

NOMENCLATURE

a weighting factors in discretized equations
c dimensionless specific heat, $\rho C_P/(\rho C_P)^*$
C_P specific heat [J kg^{-1} K^{-1}]
E a point defined in Fig. 2
E_i total thermal resistance in the interval [P, E]
f dimensionless latent heat or fraction of liquid inside a control volume, $(H-\Lambda)/\Delta H$
H total enthalpy [J kg^{-1}], $H=\Lambda$ if $T<T_f$ and $H=\Lambda+\Delta H$ if $T>T_f$
h grid size, $h=\Delta x=\Delta y$
K thermal conductivity [W m^{-1} K^{-1}]
k dimensionless thermal conductivity, K/K^*
L length of the mold [m]
N a point defined in Fig. 2
N_j total thermal resistance in the interval [P, N]
P point (x_i, y_j)
PCM phase change material
R_c thermal contact resistance at the mold–casting interface [m^2 K W^{-1}]
r_c dimensionless thermal contact resistance, R_cK^*/h
S a point defined in Fig. 2
s aspect ratio
S_j total thermal resistance in the interval [S, P]
Ste Stefan number, $C_P^*(T_0-T_\infty)/\Delta H$
T temperature [K]
t time [s]
T_f freezing point of the PCM [K]
T_0, T_∞ initial and ambient temperature [K], $T_\infty<T_f<T_0$
W a point defined in Fig. 2
W_i total thermal resistance in the interval [W, P]
w ratio of the hatched region to the size of control volume B, see Fig. 3
X, Y coordinates [m]
x, y dimensionless coordinates, $x=X/L$ and $y=Y/L$.

Greek symbols
α thermal diffusivity [m^2 s^{-1}]
ΔH latent heat of the PCM [J kg^{-1}]
Δx, Δy mesh size of the grid system
$\Delta\tau$ time step
θ dimensionless temperature, $(T-T_\infty)/(T_0-T_\infty)$
θ_f dimensionless freezing point, $(T_f-T_\infty)/(T_0-T_\infty)$
Λ sensible heat [J kg^{-1}], $\int_{T_f}^{T} C_P\,dT$
ρ density [kg m^{-3}]
σ $Ste/(1+Ste)$
τ dimensionless time, $t\,\sigma\alpha^*/L^2$.

Superscripts
* thermophysical properties of the liquid PCM at its freezing point T_f^+.

Subscripts
0 quantities at previous time step, $\tau-\Delta\tau$
c chill block
E, N, S, W points E, N, S and W, respectively
i, j quantities at point $P(x_i, y_j)$
m mold
P point P
R right-hand side of an algebraic equation.

total thermal resistances between two adjacent grid points. Hence, the arbitrary shape and the thermal contact resistance at the mold–casting interface can be easily treated without the need of coordinate transformation or grid generation. This seems to be the unique feature of the weighting function scheme. In the present study, the weighting function scheme [10] is employed to solve the solidification process of an arbitrarily shaped phase-change-material (PCM) inside a rectangle mold. For simplicity, the PCM is assumed to have a distinct freezing point. The latent heat evolved from each control volume during the solidification process is rigorously evaluated by using the enthalpy formulation proposed in ref. [10]. This enthalpy method has been proven to provide both good numerical stability and accuracy elsewhere [10]. Numerical results of the moving solidification fronts inside the PCM are presented under various parameters. The effects due to the use of chill blocks are also investigated.

THEORETICAL ANALYSIS

In many casting problems, the molds possess simple external shapes such as a cylinder, cube or rectangular parallelepiped, even though the casting is arbitrarily shaped inside. In the present investigation, a typical two-dimensional mold–casting system of this type as shown in Fig. 1 is studied. The size of the mold is $0\leqslant X\leqslant L$ and $0\leqslant Y\leqslant 0.75L$. The rectangular uniform mesh system of 97×73 grid points provided in Fig. 1 is employed for the present computations. For

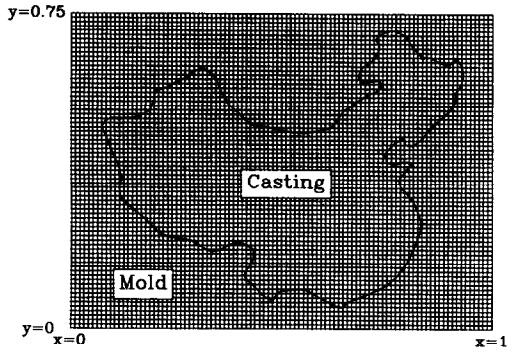

FIG. 1. A typical mold–casting system with a Cartesian grid system of 97 × 73 grid points.

simplicity, it is assumed that the cavity is initially filled with a superheated PCM at a uniform temperature T_0, while the mold is at the ambient temperature T_∞ that is below the freezing point of the PCM. Solidification thus starts from the mold–casting interface toward the centroid (roughly) of the casting as time elapses. During the solidification process, the outer surface of the mold is maintained at the ambient temperature T_∞. The natural convection inside the liquid phase of the casting is assumed negligible.

After imposing these assumptions and introducing the following dimensionless variables

$$x = X/L \quad y = Y/L \quad k = K/K^* \quad c = \rho C_P/(\rho C_P)^*$$
$$Ste = C_P^*(T_0 - T_\infty)/\Delta H \quad \theta = (T - T_\infty)/(T_0 - T_\infty)$$
$$\sigma = Ste/(1+Ste) \quad \tau = t\sigma\alpha^*/L^2 \qquad (1)$$

the energy conservation equations in the casting and the mold are expressible, respectively, as

$$(1-\sigma)\frac{\partial f}{\partial \tau} + \sigma c\frac{\partial \theta}{\partial \tau} = \frac{\partial}{\partial x}\left(k\frac{\partial \theta}{\partial x}\right) + \frac{\partial}{\partial y}\left(k\frac{\partial \theta}{\partial y}\right) \qquad (2)$$

$$c_m\frac{\partial \theta}{\partial \tau} = \frac{\partial}{\partial x}\left(k_m\frac{\partial \theta}{\partial x}\right) + \frac{\partial}{\partial y}\left(k_m\frac{\partial \theta}{\partial y}\right) \qquad (3)$$

where the subscript 'm' appearing in equation (3) denotes the thermophysical properties of the mold. The associated initial and boundary conditions are

$$\theta(x,y,0) = 1 \quad \text{inside the casting}$$
$$\theta(x,y,0) = 0 \quad \text{inside the mold}$$
$$\theta(0,y,\tau) = \theta(1,y,\tau) = 0$$
$$\theta(x,0,\tau) = \theta(x,s,\tau) = 0. \qquad (4)$$

In the dimensionless transformation (1), the superscript '*' denotes the thermophysical properties of the liquid phase of the PCM at its freezing point T_f^+. As suggested by Lee and Tzong [10], the dimensionless time τ is defined in terms of the Stefan number. Such a treatment has been proven to provide good numerical stability [10].

It is noteworthy that equation (2) covers the entire PCM including the liquid–solid interface. This has been proven by Shamsundar and Sparrow [1] and Voller and co-workers [4, 5]. The two terms on the left-hand side of equation (2) are the changing rates of the latent heat and the sensible heat during the solidification process. They are split from the total enthalpy H (i.e. $H = \Lambda$ if $T < T_f$ and $H = \Lambda + \Delta H$ if $T > T_f$). The symbol f is the dimensionless latent heat $(H-\Lambda)/\Delta H$. Its value is unity in the liquid phase and zero in the solid phase. Thus, f stands also for the fraction of liquid phase. More information on this particular enthalpy formulation can be found in ref. [10].

The energy conservation for the mold is a conventional transient heat conduction problem as presented in equation (3). In addition to equations (2)–(4), there could be a thermal contact resistance between the mold and the casting. As mentioned earlier, an air gap forms at the mold–casting interface due to the contraction of the casting and the expansion of the mold. The formation of an air gap significantly decreases the heat transfer rate from casting to mold. Hence, the thermal contact resistance at the mold–casting interface cannot be neglected in practical applications. Unfortunately, very little information is available on the growth, distribution and size of the air gap during the solidification process. Isaac *et al.* [17, 18] estimated the thermal contact resistance from the directly measured air gap. Similar attempts were also undertaken by Flach and Ozisik [19, 20] based on known temperature data at a few locations inside the solids. The air gap for castings of rectangular shape as studied by Isaac *et al.* [17, 18] was found essentially increasing as time elapsed. However, this may not be true for a complex casting as illustrated in Fig. 1. No air gap is expected in a region where the casting has a cavity with a small mouth (see the location indicated by C in Fig. 7 for example). Hence, the thermal contact resistance of refs. [17–20] cannot be directly applied on the present problem. More studies on the variations of thermal contact resistance are needed. The purpose of this paper is to propose a numerical technique that efficiently solves the solidification of arbitrarily shaped casting in mold–casting system. Although the present methodology handles the variable thermal contact resistance without difficulties, constant thermal contact resistance is assumed in the present computations due to the lack of reliable information.

NUMERICAL SOLUTION METHOD

Equations (2)–(4) constitute a conjugate heat transfer problem for the mold–casting system. Equation (2) is for the casting, while equation (3) applies to the mold. As demonstrated in Fig. 1, a uniform Cartesian grid system (x_i, y_j) with $x_i = (i-1)h$ and $y_j = (j-1)h$ is employed for the entire physical domain, where $h = \Delta x = \Delta y$ is the step size. Figure 2 shows a grid point $P(x_i, y_j)$ and its four neighbors (points W, E, S and N) with E denoting east, etc. The dashed lines are the boundaries of the control volume of point P. This

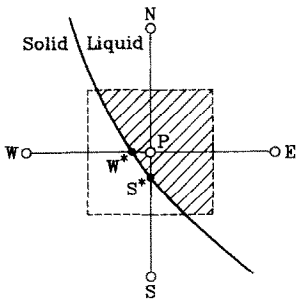

FIG. 2. A solidification front passing through a control volume.

control volume will be referred to as 'the control volume P' in the present study for simplicity.

If all of the five points and the control volume P are located in the casting, then equation (2) can be discretized by using the weighting function scheme proposed in ref. [10]. This leads to the algebraic equation for pure heat conduction case

$$a_W\theta_{i-1,j}+a_E\theta_{i+1,j}+a_S\theta_{i,j-1}+a_N\theta_{i,j+1}+a_P\theta_{i,j}=a_R \tag{5}$$

$$a_W=h/W_i \quad a_E=h/E_i \quad a_S=h/S_j \quad a_N=h/N_j$$

$$a_P=-a_W-a_E-a_S-a_N-\sigma c_{i,j}h^2/\Delta\tau$$

$$a_R=(h^2/\Delta\tau)[(1-\sigma)(f-f_0)_{i,j}-\sigma(c\theta_0)_{i,j}] \tag{6}$$

where the subscript '0' denotes quantities at the previous time ($\tau_0=\tau-\Delta\tau$) and

$$W_i=\int_{x_{i-1}}^{x_i}\frac{1}{k}\,dx \quad E_i=\int_{x_i}^{x_{i+1}}\frac{1}{k}\,dx$$

$$S_j=\int_{y_{j-1}}^{y_j}\frac{1}{k}\,dy \quad N_j=\int_{y_j}^{y_{j+1}}\frac{1}{k}\,dy. \tag{7}$$

It appears that the quantities W_i, E_i, S_j and N_j defined in equations (7) are, respectively, the overall thermal resistances in the intervals [W, P], [P, E], [S, P] and [P, N]. Due to the lack of detailed information about the variation of the thermal conductivity k between two adjacent grid points, the thermal resistance $1/k$ is assumed to have a linear variation in each of the intervals. Hence

$$a_W=2k_Wk_P/(k_W+k_P)$$

$$a_E=2k_Ek_P/(k_E+k_P)$$

$$a_S=2k_Sk_P/(k_S+k_P)$$

$$a_N=2k_Nk_P/(k_N+k_P). \tag{8}$$

However, for most PCM, the thermal conductivity of the solid phase is quite different from that of the liquid phase. Thus, equations (8) would not be true if the solidification front is located inside the control volume P as illustrated in Fig. 2. Suppose the solidification front intersects the line $\overline{WP}$ at point W* and the line $\overline{SP}$ at point S*, i.e. $\theta_W^*=\theta_S^*=\theta_f$. Under such a situation, the overall thermal resistance in [W, P] should be evaluated from

$$W_i=\int_W^P\frac{1}{k}\,dx=\int_W^{W^*}\frac{1}{k}\,dx+\int_{W^*}^P\frac{1}{k}\,dx. \tag{9}$$

The assumption of linear thermal resistance variation in each of the subintervals [W, W*] and [W*, P] yields

$$a_W=2(1-\gamma)k_Wk(\theta_f^-)/(k_W+k(\theta_f^-))+2\gamma k_Pk(\theta_f^+)/(k_P+k(\theta_f^+)) \tag{10}$$

where $\gamma=\overline{W^*P}/\overline{WP}$ and the notations $k(\theta_f^-)$ and $k(\theta_f^+)$ represent the thermal conductivity at θ_f and θ_f^+. The weighting factor a_S can be evaluated in a similar manner. In case point P and its four neighbors are all located inside the mold, the discretized equations would be the same as equations (5)–(8) with $\sigma=1$.

When control volume P covers both casting and mold, the relationship among the temperatures of point P and its four neighbors would be governed by both equations (2) and (3) as well as the thermal contact resistance at the mold–casting interface. Suppose grid point A is on one side of the mold–casting interface, while one of its neighbors (point B) is on the other side as illustrated in Fig. 3. Generally speaking, the mold–casting interface would not 'happen' to coincide with the interface of two adjacent control volumes. This implies that part of control volume A (see the right upper corner, for instance) might be inside the casting, when point A is located in the mold. Under such a situation, the temperature and the thermophysical properties of this particular part could be very different from that of point A, especially when the thermal contact resistance is large at the mold–casting interface. Hence, the latent heat and sensible heat evolved from this part during the solidification process should not be treated as heat generation from point A. In the present study, this energy evolution is regarded as that belonging to control volume B. The sensible heat released from the mold region covered by control volume B (see the left lower corner of control volume B) is treated similarly. As a result, all of the energy evolution from the hatched region as shown in Fig. 3 is regarded as heat generation from control volume B. Based on this

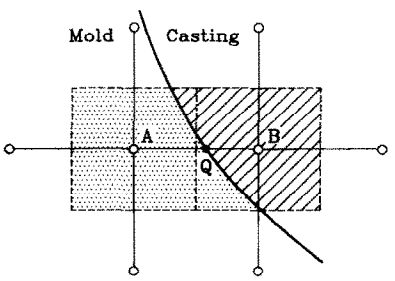

FIG. 3. Two adjacent control volumes covering both the mold and the casting.

assumption, the discretized energy equation for point $B(x_i, y_j)$ is expressible as

$$(a_W)_B\theta_{i-1,j}+(a_E)_B\theta_{i+1,j}+(a_S)_B\theta_{i,j-1}+(a_N)_B\theta_{i,j+1}+(a_P)_B\theta_{i,j}=(a_R)_B \quad (11)$$

$$(a_W)_B = h/W_i \quad (a_E)_B = h/E_i \quad (a_S)_B = h/S_j$$

$$(a_N)_B = h/N_j \quad (a_P)_B = -(a_W)_B-(a_E)_B-(a_S)_B-(a_N)_B-w\sigma c_{i,j}h^2/\Delta\tau$$

$$(a_R)_B = (h^2/\Delta\tau)[(1-\sigma)(f-f_0)_{i,j}-w\sigma(c\theta_0)_{i,j}] \quad (12)$$

where point P coincides with point B and the notations $(a_P)_B$, $(a_W)_B$, $(a_E)_B$, etc. represent the weighting factors when the governing equation is discretized at point B. The symbol w is the ratio of the hatched area to the area of control volume B. It could have a value of larger than unity. The f-value in equation (12) is the ratio of the liquid area inside the hatched region to the area of control volume B. This implies that the f-value is always equal to or smaller than w.

It should be noted also that there might exist a significant thermal contact resistance at the mold–casting interface. Thus, care must be exercised in computing the integrations in equations (7). Let Q be the intersection point of the mold–casting interface and the line $\overline{AB}$. From equation (7), the overall thermal resistance W_i can be evaluated by

$$W_i = \int_A^B \frac{1}{k}\,dx = \int_A^Q \frac{1}{k_m}\,dx + r_c + \int_Q^B \frac{1}{k}\,dx \quad (13)$$

where $r_c = R_cK^*/h$ is the dimensionless thermal contact resistance at the mold–casting interface (point Q). The overall thermal resistance S_j in the interval lying to the south of point B can be determined similarly. The algebraic equation for point A is the same as that for point B (equations (11) and (12)) with $\sigma = 1$ and w being the ratio of the dotted area (see Fig. 3) to the area of control volume A. Due to the assumption of no natural convection effect, the weighting factors $(a_E)_A$ and $(a_W)_B$ have the same value.

After discretizing the governing equations on each of the grid points and imposing the boundary conditions, one obtains a system of algebraic equations in the matrix form

$$[A]\{\theta\} = \{\mathbf{B}\} \quad (14)$$

where $[A]$ is a square matrix of order M and $\{\mathbf{B}\}$ is an M dimensional vector with M being the total number of grid points. In the present study, M has a value as large as $97 \times 73 = 7081$. Fortunately, the coefficient matrix $[A]$ has only five nonzero diagonals. Hence, equation (14) can be efficiently solved by employing the SIS solver [21]. The numerical procedure is essentially the same as that presented in ref. [10] for the case without mold.

RESULTS AND DISCUSSION

Numerical results were obtained for the mold–casting system as shown in Fig. 1 under various important parameters such as Stefan number (*Ste*), thermal contact resistance at mold–casting interface (r_c) and thermophysical property of the mold (k_m and c_m). The effects due to the use of chill blocks were also investigated. The present study emphasizes the effects of thermophysical properties of the mold on the solidification process. In addition, the effects of temperature-dependent thermophysical properties of the casting have been studied in detail in refs. [10, 22]. Hence, the thermophysical properties were assumed constant inside the entire casting including both liquid and solid phases for convenience. For simplicity, the dimensionless freezing point $\theta_f = 0.8$ was used for all of the cases studied in the present investigation.

Figure 4 presents the solidification fronts at each time step under the parameters, $Ste = 5$, $r_c = 0$, $k_m = 2$, $c_m = 2$ and the time step $\Delta\tau = 0.002$. The solid curves are the solidification fronts obtained by using the grid size of $h = 1/96$, while the dashed curves are based on a coarser grid $h = 1/48$. Thanks to the use of the particular enthalpy formulation proposed in ref. [10], the numerical results of solidification front possess smooth profiles as observable from Fig. 4. From the solid curves, it is seen that the solidification front at each time step forms an enclosed curve. It moves inward from the mold–casting interface to a location near the centroid of the casting. At the very beginning of the solidification process, the freezing rate of the casting is quite fast due to large temperature difference. Such a situation is particularly pronounced at the northeast corner of the casting where the surface to volume ratio is large. This is consistent with the physical reasoning.

From a comparison between the solid and dashed curves shown in Fig. 4, the numerical results are seen to change only a little even if the grid size is doubled. In the case of the coarse grid system, however, there would be not enough grid points to handle the profile of the solidification front when the casting is about to completely solidify. Hence, a heavy underrelaxation

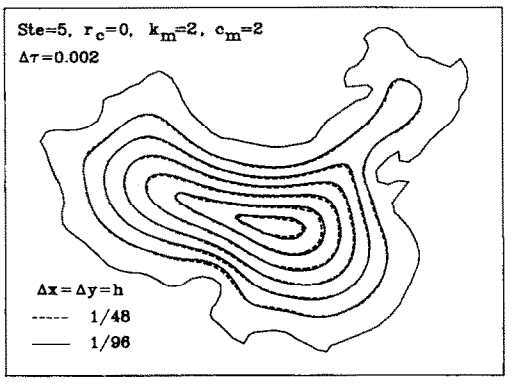

FIG. 4. Influence of grid size on solidification fronts (with time increment 0.002) for $Ste = 5$, $r_c = 0$, $k_m = 2$, $c_m = 2$.

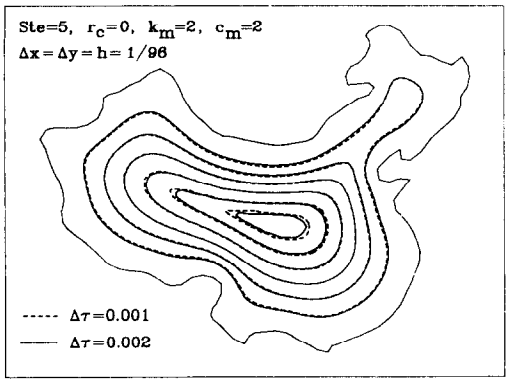

FIG. 5. Influence of time step size on the solidification fronts (with time increment 0.002) for $Ste = 5$, $r_c = 0$, $k_m = 2$, $c_m = 2$.

factor (small SOR) is generally needed for a better solution convergence rate. To achieve both high resolution and good numerical stability, the grid system with the step size $h = 1/96$ (see Fig. 1) is used hereafter in the present study.

To examine the influence of the time step $\Delta\tau$ on the resulting solidification front, the same problem as in Fig. 4 is resolved on a smaller time step ($\Delta\tau = 0.001$). The result is represented by the dashed curves in Fig. 5 with a time-increment of 0.001. The result based on $\Delta\tau = 0.002$ is also presented in Fig. 5 with solid curves for comparison. It appears from Fig. 5 that the numerical result based on the present method is not sensitive to the time step. In fact, a larger time step would provide a better numerical stability in the use of the present enthalpy method. For instance, in the present case, the optimum successive over-relaxation factor is about SOR = 0.2 for $\Delta\tau = 0.002$ as compared to SOR = 0.1 for $\Delta\tau = 0.001$. This important feature of the present enthalpy formulation has been well-discussed in refs. [10, 22].

Figure 6 shows the numerical result of solidification fronts in the case when the Stefan number is decreased to $Ste = 1$, while all of other parameters are maintained the same as in Fig. 4. As defined in equation (1), the Stefan number stands for the relative importance of sensible heat and latent heat. A small Stefan number means large latent heat. Thus, in the case with a small Stefan number it is expected that the casting will take longer to completely solidify. This can be clearly seen by comparing the solidification front in Fig. 6 with that in Fig. 4. For instance, the total solidification time is $\tau = 0.0210$ ($t = 0.0420L^2/\alpha^*$) for $Ste = 1$ as compared to $\tau = 0.0121$ ($t = 0.0145L^2/\alpha^*$) for $Ste = 5$. In the case of a small Stefan number, when the solidification is going to finish, the entire liquid 'pool' would be essentially isothermal due to large latent heat evolution. For example, for the case of $Ste = 1$, the maximum temperature in the liquid phase is $\theta_{max} = 0.8051$ at $\tau = 0.012$, that is, only slightly higher than the freezing point $\theta_f = 0.8$. Under such a situation, the location of the solidification front is very difficult to identify from the temperature solution. This interpolation error might have produced the sinuous profiles for the solidification front at $\tau > 0.012$ as observable from Fig. 6.

The solidification fronts based on the parameters $Ste = 5$, $r_c = 1$, $k_m = 2$, $c_m = 2$ are presented in Fig. 7. This set of parameters is the same as that in Fig. 4 except for the thermal contact resistance $r_c = 1$. The time step used in the computations is $\Delta\tau = 0.01$. Like an insulator along the boundary of the casting, the thermal contact resistance prevents the conduction of heat from the casting to the mold. Thus, heat accumulates along the boundary of the casting such that the occurrence of solidification is depressed especially at the concave boundaries indicated by A, B and C where the casting has a small surface to volume ratio. This might account for the fact that solidification occurs only at some convex corners of the casting at the beginning stage of the casting process. Due to this situation, the solidification front could intersect the mold–casting interface (see the solidification front labeled 'b' for example). This characteristic is different from that of Fig. 4, a case without thermal contact resistance. Physically speaking, without the 'protection' of thermal contact resistance, the initial temperature jump ($T_0 - T_\infty$) at the mold–casting interface would start the solidification immediately along the

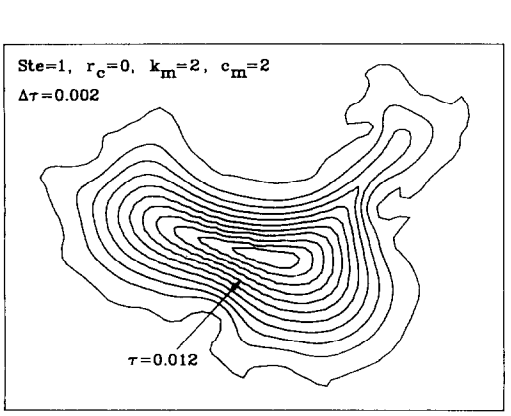

FIG. 6. Solidification fronts with time increment 0.002 for $Ste = 1$, $r_c = 0$, $k_m = 2$, $c_m = 2$.

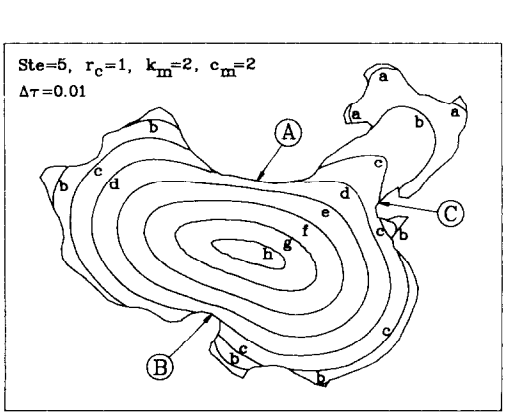

FIG. 7. Solidification fronts with time increment 0.01 for $Ste = 5$, $r_c = 1$, $k_m = 2$, $c_m = 2$.

boundaries of the casting. As a result, the solidification front is essentially parallel to the mold–casting interface at the beginning stage of solidification process as observable from Fig. 4. From Fig. 7, the thermal contact resistance $r_c = 1$ is seen to increase the total solidification time from $\tau = 0.0121$ ($t = 0.0145L^2/\alpha^*$) to $\tau = 0.0824$ ($t = 0.0988L^2/\alpha^*$) as expected.

Slow solidification rate can also be encountered when the mold has poor thermal conductivity and/or specific heat. To clarify this point, the solidification fronts based on $Ste = 5$, $r_c = 0$, $k_m = 0.2$, $c_m = 0.5$ are shown in Fig. 8. The time step used in the computations was $\Delta\tau = 0.005$. From Fig. 8, it is seen that the total solidification time increases to $\tau = 0.0456$ ($t = 0.0548L^2/\alpha^*$) due to the poor thermophysical properties of the mold. However, the characteristics of the solidification fronts in Fig. 8 are different from those in Fig. 7 in some respects. Due to the lack of thermal contact resistance, the solidification front in Fig. 8 is roughly parallel to the boundary of the casting as in Fig. 4. However, heat might also accumulate at the strongly-concave boundaries, if the thermal conductivity of the mold is sufficiently small. Such a phenomenon can be found in the regions indicated by A, B and C in Fig. 8.

From Figs. 7 and 8, it appears that solidification near the concave boundaries of the casting might be depressed if the mold has either poor thermophysical properties or large thermal contact resistance. This situation would result in casting defects on the concave surfaces of the casting. Unfortunately, such a difficulty is encountered in many sand casting processes. One popular method in foundry technology is to put chill blocks inside the mold to improve the solidification rate near the concave surface of the casting. Figure 9 reveals the solidification fronts under the effects of three chill blocks that possess good thermophysical properties ($k_c = 5$ and $c_c = 2$). The locations of these chill blocks are shown also in Fig. 9. In the computations, all of the physical parameters are the same as that in Fig. 8. From Fig. 9, one sees that the solidification rate near the concave surfaces

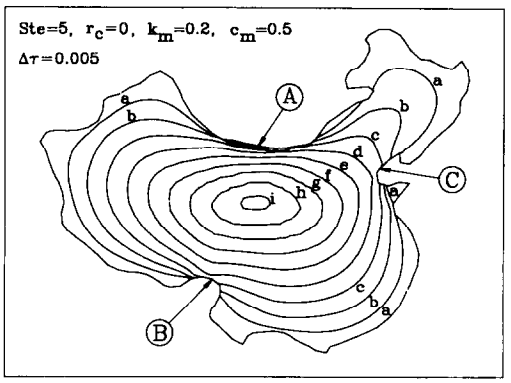

FIG. 8. Solidification fronts with time increment 0.005 for $Ste = 5$, $r_c = 0$, $k_m = 0.2$, $c_m = 0.5$.

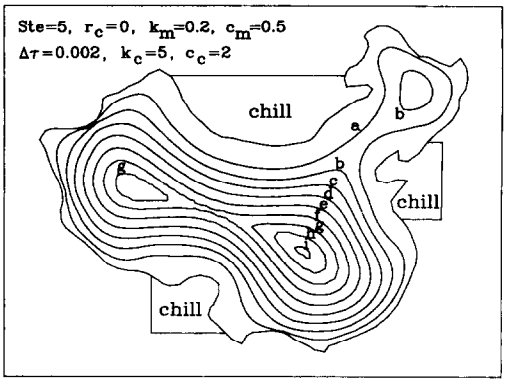

FIG. 9. Effect of chill blocks on solidification fronts (with time increment 0.002) for $Ste = 5$, $r_c = 0$, $k_m = 0.2$, $c_m = 0.5$, $k_c = 5$, $c_c = 2$.

is significantly improved by the chill blocks. In addition, the total solidification time is reduced significantly from $\tau = 0.0456$ without chill to $\tau = 0.0182$ with chills. During some time intervals, the liquid phase separates into two isolated regions due to the effect of chill blocks as observable from the curves labeled 'b' and 'g' in Fig. 9. The present numerical technique seems to pose no numerical difficulty for this 'multiple-region' problem.

CONCLUSION

An efficient enthalpy formulation developed previously was employed in the present study for an arbitrarily shaped casting in mold–casting system. A particular treatment on the evolution of the latent heat was proposed for grid cells covering both mold and casting. Thanks to the use of the weighting function scheme, all of the computations could be performed in the conventional Cartesian coordinates without recourse to coordinate transformation or grid generation. In addition, the weighting function scheme was found to solve the conjugate mold–casting system quite efficiently even in the presence of thermal contact resistance at the mold–casting interface. From the numerical results, it is seen that for a casting having large latent heat, quite a long time would be needed for the casting to completely solidify. In the presence of thermal contact resistance, heat accumulates along the boundary of the casting such that solidification occurs only at some convex corners of the casting at early stage of the process. As expected, both thermal contact resistance and the use of a mold with poor thermophysical properties depress the solidification rate. However, their solidification fronts show different characteristics. When either the mold has poor thermophysical properties or the thermal contact resistance is large, serious heat accumulation would occur on the concave surface of the casting. This undesirable situation can be improved by the use of chill blocks. Under some conditions, the liquid phase might separate into two or more isolated

regions. The present numerical technique solves such a problem as well.

Acknowledgements—The authors wish to express their appreciation to the National Science Council of the Republic of China in Taiwan for the financial support of this work through the project NSC80-0401-E007-12.

REFERENCES

1. N. Shamsundar and E. M. Sparrow, Analysis of multidimensional conduction phase change via the enthalpy model, *ASME J. Heat Transfer* **97,** 333–340 (1975).
2. G. E. Schneider and M. J. Raw, An implicit solution procedure for finite difference modeling of the Stefan problem, *AIAA J.* **22,** 1685–1690 (1984).
3. G. E. Schneider, Computation of heat transfer with solid/liquid phase change including free convection, *AIAA J. Thermophysics Heat Transfer* **1,** 136–145 (1987).
4. V. R. Voller, Interpretation of the enthalpy in a discretized multidimensional region undergoing a melting/freezing phase change, *Int. Commun. Heat Mass Transfer* **10,** 323–328 (1983).
5. V. R. Voller, M. Cross and N. C. Markatos, An enthalpy method for convection/diffusion phase change, *Int. J. Numer. Meth. Engng* **24,** 271–284 (1987).
6. W. D. Bennon and F. P. Incropera, A continuum model for momentum, heat and species transfer in binary solid–liquid phase change systems—I. Model formulation, *Int. J. Heat Mass Transfer* **30,** 2161–2170 (1987).
7. W. D. Bennon and F. P. Incropera, A continuum model for momentum, heat and species transfer in binary solid–liquid phase change systems—II. Applications to solidification in a rectangular cavity, *Int. J. Heat Mass Transfer* **30,** 2161–2170 (1987).
8. G. E. Bell, On the performance of the enthalpy method, *Int. J. Heat Mass Transfer* **25,** 587–589 (1982).
9. N. Shamsundar and E. Rooz, Numerical methods for moving boundary problems. In *Handbook of Numerical Heat Transfer*, Ch. 18, pp. 760–763. Wiley, New York (1988).
10. S. L. Lee and R. Y. Tzong, An enthalpy formulation for phase change problems with a large thermal diffusivity jump across the interface, *Int. J. Heat Mass Transfer* **34,** 1491–1502 (1991).
11. P. G. Kroeger and S. Ostrach, The solution of a two-dimensional freezing problem including convection effects in the liquid region, *Int. J. Heat Mass Transfer* **17,** 1191–1207 (1974).
12. S. D. Gilmore and S. I. Guceri, Solidification in anisotropic thermoplastic composites, *Polymer Composites* **11,** 406–416 (1990).
13. K. Davey and S. Hinduja, Modelling the transient thermal behavior of the pressure die-casting process with the BEM, *Appl. Math. Modelling* **14,** 394–409 (1990).
14. R. J. Kelly, Solidification of the candidate hammer casting using C.A.S.T. In *Modelling of Casting and Welding Process IV* (Edited by A. F. Giamei and G. J. Abbaschian), pp. 789–803. The Minerals, Metals and Materials Society, Pennsylvania (1988).
15. K. Anzai, T. Uchida and E. Niyama, Solidification simulation and calculation using the HICASS casting CAD system. In *Modelling of Casting and Welding Process IV* (Edited by A. F. Giamei and G. J. Abbaschian), pp. 805–816. The Minerals, Metals and Materials Society, Pennsylvania (1988).
16. P. N. Hansen and P. R. Sahm, Modeling the solidification process in a steel hammer casting using the GEOMESH software system. In *Modelling of Casting and Welding Process IV* (Edited by A. F. Giamei and G. J. Abbaschian), pp. 817–823. The Minerals, Metals and Materials Society, Pennsylvania (1988).
17. J. Isaac, G. P. Reddy and G. K. Sharma, Experimental investigation of the influence of casting parameters on the formation and distribution of air gap during the solidification of castings in metallic molds, *AFS Trans.* **93,** 29–34 (1985).
18. J. Isaac, G. P. Reddy and G. K. Sharma, Variations of heat transfer coefficients during solidification of castings in metallic moulds, *The British Foundryman* **78,** 465–468 (1985).
19. G. P. Flach and M. N. Ozisik, Periodic B-spline basis for quasi-steady periodic inverse heat conduction, *Int. J. Heat Mass Transfer* **30,** 869–880 (1987).
20. G. P. Flach and M. N. Ozisik, Inverse heat conduction problem of periodically contacting surfaces, *ASME J. Heat Transfer* **110,** 821–829 (1988).
21. S. L. Lee, A strongly implicit solver for two-dimensional elliptic differential equations, *Numer. Heat Transfer* **16B,** 161–178 (1989).
22. W. Y. Raw and S. L. Lee, Application of weighting function scheme on convection–conduction phase change problems, *Int. J. Heat Mass Transfer* **34,** 1503–1513 (1991).

SOLIDIFICATION D'UNE COULEE DANS UN MOULE DE FORME QUELCONQUE

Résumé—On applique la formulation enthalpique au mécanisme de solidification d'une coulée de forme arbitraire dans un moule. L'effet de résistance thermique de contact à l'interface moule-coulée est aussi étudié. On conduit les calculs dans un système de coordonnées rectangulaires sans recours à une transformation de coordonnées ou à une génération de grille pour une forme arbitraire de l'interface. On considère quelques cas pour étudier les effets du nombre de Stefan, des propriétés thermophysiques et de la résistance thermique de contact sur l'évolution de la solidification. Les résultats numériques sur le front mobile de solidification sont étudiés dans chaque cas. On considère des blocs refroidisseurs en quelques endroits dans le moule de façon qu'il puisse exister plusieurs régions liquides isolées pendant le mécanisme de solidification. Même pour un tel problème 'multi-région', la méthode numérique présente montre de bonnes performances; il n'y a pas besoin d'effort supplémentaire de calcul pour traiter le cas par rapport au cas sans bloc refroidisseur.

ERSTARRUNGSVORGANG EINES BELIEBIG GEFORMTEN GUSSTEILS IN EINEM FORM–GUSSTEIL-SYSTEM

Zusammenfassung—In der vorliegenden Arbeit wird ein Enthalpie-Verfahren auf den Erstarrungsvorgang eines beliebig geformten Gußteils in einem Form–Gußteil-System angewandt. Außerdem wird der Einfluß des thermischen Kontaktwiderstands an der Grenzfläche zwischen Form- und Gußteil untersucht. Alle Berechnungen werden in kartesischen Koordinaten durchgeführt, trotz der willkürlichen Form der Grenzfläche. Ein Einzonen-Modell ist zusammen mit Gewichtungsfunktionen in der Lage, das konjugierte Wärmeübertragungsproblem effizient zu lösen. In einigen Fällen wird der Einfluß der Stefan-Zahl, der thermophysikalischen Stoffeigenschaften und des Kontaktwiderstands (an der Form–Gußteil-Grenzfläche) auf den Erstarrungsvorgang untersucht. Das numerische Ergebnis für die bewegliche Erstarrungsfront wird für jeden Fall betrachtet. Um die Übereinstimmung der eingesetzten Numerik in einem ganz bestimmten Fall zu untersuchen, werden Kühlsteine in der Form verteilt, so daß mehr als eine Flüssigkeitsregion während der Erstarrung auftreten kann. Sogar für solche Mehrzonen-Probleme zeigt die numerische Methode gutes Verhalten. Verglichen mit den Fällen ohne Abkühlsteine sind keine zusätzlichen Berechnungen notwendig.

ЗАТВЕРДЕВАНИЕ ОТЛИВКИ ПРОИЗВОЛЬНОЙ ФОРМЫ В СИСТЕМАХ КОКИЛЬ-ОТЛИВКА

Аннотация—В настоящем исследовании уравнение для энтальпии применяется при описании процесса затвердевания отливки произвольной формы в системе кокиль–отливка. Рассматривается также влияние теплового контактного сопротивления на границе раздела кокиль–отливка. Все расчеты проводятся в декартовой системе координат без перехода к новым координатам и без образования сетки для произвольной формы границы раздела. Показано, что сопряженная задача теплопереноса в системе кокиль–отливка решается с использованием схемы весовых функций. Исследуется влияние числа Стефана, теплофизических свойств и теплового контактного сопротивления (на границе раздела) на процесс затвердевания для нескольких случаев. В каждом из них численно определяется положение движущегося фронта затвердевания. С целью исследования эффективности предложенного численного метода проведены расчеты для случая использования кокильных блоков, расположенных в кокиле таким образом, что при отливке в процессе затвердевания могут присутствовать более чем один жидкий участок. Показано, что представленный численный метод эффективен даже для решения такой задачи, при этом не возикает необходимость дополнительных расчетов по сравнению со случаями отсутствия кокильных блоков.